Shock Waves (2000) 10: 33–41

Shock Waves


# Numerical simulation of detonation reignition in $H_2$-$O_2$ mixtures in area expansions

D.A. Jones[1], G. Kemister[1], N.A. Tonello[2,*], E.S. Oran[3], M. Sichel[4]

[1] Aeronautical and Maritime Research Laboratory, DSTO, PO Box 4331, Victoria 3001, Australia
[2] CRAFT, Tech., 174 North Main Street, Bldg. 3, PO Box 1150, Dublin, PA 18917, USA
[3] Laboratory for Computational Physics and Fluid Dynamics, Naval Research Laboratory, Code 6404, Washington, DC 20375, USA
[4] Department of Aerospace Engineering, University of Michigan, Ann Arbor, MI 48109-2140, USA

Received 16 July 1998/ Accepted 17 November 1998

**Abstract.** Time-dependent, two-dimensional, numerical simulations of a transmitted detonation show reignition occuring by one of two mechanisms. The first mechanism involves the collision of triple points as they expand along a decaying shock front. In the second mechanism ignition results from the coalescence of a number of small, relatively high pressure regions left over from the decay of weakened transverse waves. The simulations were performed using an improved chemical kinetic model for stoichiometric $H_2$-$O_2$ mixtures. The initial conditions were a propagating, two-dimensional detonation resolved enough to show transverse wave structure. The calculations provide clarification of the reignition mechanism seen in previous $H_2$-$O_2$-Ar simulations, and again demonstrate that the transverse wave structure of the detonation front is critical to the reignition process.

**Key words:** Detonation reignition, $H_2$-$O_2$ detonations, Multidimensional detonation dynamics, Transmitted detonations

## 1 Introduction

Detonation transmission between explosive layers has been studied experimentally by Liu et al. (1987, 1988) and Tonello et al. (1995) using a special, layered-detonation tube. Schlieren photography was used to visualize the interactions which occur between the primary detonation and a bounding explosive mixture. When the explosive mixture in the two layers is the same, the diffraction of the primary detonation is identical to that which occurs at an area expansion. The experiments showed that ignition of the secondary explosive can be induced either by shock reflection from the confining walls, or by direct reignition of the explosive as the shock wave from the detonation in the primary explosive expands into the secondary explosive. In the direct-ignition case, the schlieren photographs show that the shock front and the reaction front in the secondary explosive initially separate and the detonation begins to fail. At some stage, an explosion occurs in the shock-heated material between the shock front and the reaction. This explosion produces a strongly coupled reactive shock wave which travels along the curved leading shock and reignites the detonation.

The mechanism involved in this process is related to the transverse waves in the detonation front. Even a thin 30 nm collodion film separating the primary and bounding mixture was able to block this process (Liu et al. 1988). Jones et al. (1996) performed numerical simulations of these experiments for a mixture of $H_2$-$O_2$ heavily diluted with Ar and showed that direct reignition fails when the transverse waves in the detonation in the primary explosive are suppressed, as also observed experimentally. Tonello et al. (1996) repeated these calculations for a stoichiometric $H_2$-$O_2$ mixture with a more accurate chemical model, still not resolving transverse waves, and again did not observe direct reignition. However, when Jones et al. (1996) resolved the transverse wave structure for $H_2$-$O_2$-Ar the simulations showed direct reignition of the detonation in the secondary explosive. The form of this reignition showed striking similarities to the reignition seen experimentally in undiluted $H_2$-$O_2$ mixtures.

In this paper we describe recent simulations using the improved chemical kinetic model of Tonello for stoichiometric $H_2$-$O_2$ mixtures. These highly resolved computations are initiated by detonations with an existing transverse wave structure. The calculations provide further insight and clarification of the reignition mechanism seen

*Correspondence to*: M. Sichel (e-mail: sichel@umich.edu)
* *Present address:* Computational Dynamics Ltd., 200 Shepherds Bush Road, London W6 7NY, UK
An abridged version of this paper was presented at the 16th Int. Colloquium on the Dynamics of Explosions and Reactive Systems at Krakow, Poland, from July 27 to August 1, 1997

in the previous $H_2$-$O_2$-Ar simulations, and again demonstrate that the transverse wave structure of the detonation front is critical to the reignition process. We show that reignition occurs by one of two mechanisms, depending on the initial conditions of the simulation. The first mechanism is similar to that observed in $H_2$-$O_2$-Ar by Jones et al. (1996) and involves the collision of triple points as they expand along the decaying shock front. In the second mechanism ignition occurs as a result of the coalescence of a number of small hot spots. These are formed by the interaction of relatively high pressure regions left over from the decay of weakened transverse waves.

## 2 The chemical model

Numerical simulations of detonation require solutions of the reactive Euler equations. For the stoichiometric $H_2$-$O_2$ system considered here, the ideal approach entails solving all the individual species conservation equations, integrating all the rate equations which form the $H_2$-$O_2$ reaction mechanism, and solving equations describing the conservation of mass, momentum, and energy. While such calculations are now feasible (e.g., Weber 1994; Oran et al. 1998), the strategy is computationally very demanding and not suited to the current study. In order to simulate the two dimensional detonation problem considered here, the full kinetic mechanism is replaced by a simplified model which attempts to reproduce the major, relevant characteristics of the reacting $H_2$-$O_2$ system. In this paper, we use a two-step model in which the chemical processes are broken into two distinct phases, the induction period and the energy-release period. The induction period is an essentially thermoneutral period during which the radical pool is built up, but the reactant concentration remains approximately constant. In the second stage, significant chemical changes occur and large amounts of energy are released. In the simplest two-step models, only the energy release is taken into account, while the chemical composition is kept unchanged. Such models have been used successfully by Taki and Fujiwara (1981), Oran et al. (1992) and Jones et al. (1995) in one or two dimensional detonation problems. The main problem with these models is that the composition at the end of the reaction is wrong, and this leads to incorrect estimates of some of the gas dynamic variables. Lefebvre et al. (1992) have shown that such errors can have important consequences. They showed that more accurate results can be obtained by taking into account the chemical conversion to products and using the correct ratio of specific heats and molecular mass (Lefebvre et al. 1993).

The difference between the model used in this paper and the two-step reaction models previously used is that it takes into account the change of mixture composition during chemical reaction. The progress of the chemical reaction is described in terms of the change in chemical composition, rather than in terms of energy release. Unlike previous models, the amount of heat released does not appear in the calculations as an input parameter, but occurs as a result of the change in the composition of the mixture itself as the reaction progresses. Full details of this two-step model are described by Tonello (1996), while a brief description is provided below.

The expression for the induction time $\tau$ for a stoichiometric $H_2$-$O_2$ mixture derived by Tonello has the form

$$\ln(\tau[O_2]) = A + \frac{B}{T} + CP^n \exp\left(\frac{D}{T}\right) \qquad (1)$$

where $A = -23.6457$, $B = 8530.6$ K, $C = 7.2208 \times 10^{-11}$ $(\text{atm})^{-2}$, $D = 21205$ K, $n = 2$, and pressure is measured in atmospheres. Equation (1) has the same qualitative form as the expression derived by Meyer and Oppenheim (1971), but the coefficients have been recomputed so that the expression reproduces the induction times calculated by Burks and Oran (1981). Burks and Oran numerically integrated the equations describing the full $H_2$-$O_2$ mechanism (approximately 50 reactions) over a wide temperature and pressure range, and then checked the results by comparison with experimental data for explosion limits, induction times, and the temporal evolution of species concentrations. Equation (1) is valid for the conditions $T > 700$ K and $P > 0.1$ MPa. We also introduce an induction parameter $f$, which represents the fraction of induction time already elapsed. The quantity $f$ is obtained from the solution of the equation

$$\frac{\mathrm{d}f}{\mathrm{d}t} = \frac{1}{\tau(T,P)} \qquad (2)$$

where $f(0) = 0$. Energy release begins when $f = 1$.

The reaction time in detonation waves in $H_2$-$O_2$ is typically of the order of 1 or 2 $\mu$s (Westbrook 1982). However, because of the great sensitivity of the $H_2$-$O_2$ reaction to the pressure and temperature, it is very difficult to determine an overall rate of reaction which would be valid over a wide range. Therefore, in the absence of sound experimental or analytical data, a generic Arrhenius form has been assumed, and the influence of its parameters on the calculated results has been examined in detail. The reaction rate has the form

$$\frac{\mathrm{d}\lambda}{\mathrm{d}t} = (1-\lambda)a \times \exp\left(-\frac{b}{T}\right) + c \quad . \qquad (3)$$

The constant $c$ has been added to allow simulation of constant reaction rates. The parameter $b$ is the equivalent of an activation energy, and the constant $a$ is the pre-exponential factor, representing the collision frequency. Six different reaction rate functions were examined and these are described in Table 1. For each of these functions, the pre-exponential factor $a$ was adjusted so that the reaction time was kept equal to 2 $\mu$s, in accordance with the results cited above. The effect of each of the reaction rate expressions on the energetics of a one-dimensional detonation has been described in detail by Tonello (1996). Below we consider the effect of some of these expressions on the two-dimensional cellular detonation structure.

Equation (3) represents an overall reaction rate which defines the progress of the reaction and the species concentration at each stage of the reaction. The next problem

**Table 1.** Coefficients $a$, $b$, and $c$ for the generic Arrhenius reaction rate function

| | A | B | C | D | E | F |
|---|---|---|---|---|---|---|
| $a(\mathrm{s}^{-1})$ | $3.16 \times 10^6$ | $1.426 \times 10^7$ | $3.45 \times 10^7$ | $1.2 \times 10^8$ | $5.31 \times 10^8$ | 0.0 |
| $b(\mathrm{K})$ | 0.0 | $4.0 \times 10^3$ | $6.0 \times 10^3$ | $8.0 \times 10^3$ | $10.0 \times 10^3$ | 0.0 |
| $c(\mathrm{s}^{-1})$ | 0.0 | 0.0 | 0.0 | 0.0 | 0.0 | $5.0 \times 10^5$ |

is to relate the progress variable $\lambda$ to $Y_i$, the mass fraction of species $i$. We assume that the mixture composition changes linearly with the progress variable $\lambda$, from reactants to products, so that the mass fractions of the species are given by

$$Y_i = (Y_{i,P} - Y_{i,R})\lambda + Y_{i,R} \tag{4}$$

where $Y_{i,R}$ and $Y_{i,P}$ represent the mass fractions of the individual reactants and products. These are computed in advance using the Gordon-McBride NASA CEC71 equilibrium computer code. A total of eight species are considered in this model: $H_2$, $O_2$, H, O, $HO_2$, $H_2O$, $H_2O_2$, and OH. For a mixture of N species the specific internal energy of the mixture is given by

$$\varepsilon = \sum_{i=1}^{N} Y_i \varepsilon_i(T) \tag{5}$$

where $\varepsilon$ is the specific internal energy of the mixture and $\varepsilon_i$ is the specific internal energy of species $i$. If we assume that the mixture and its constituent species are perfect gases, then the specific internal energy of species $i$ can be expressed as a function of the enthalpy

$$\varepsilon = h_i - \frac{P_i}{\rho_i} = \frac{\bar{h}_i}{\bar{m}_i} - \frac{P_i}{\rho_i} \tag{6}$$

where $h_i$, $\rho_i$, $P_i$, and $m_i$ are the total specific enthalpy, the density, the pressure, and the molal mass of species $i$, respectively. There is a considerable amount of data available on the enthalpy of various species at different temperatures, and least squares fits are used to describe the variation of enthalpy with temperature. We use the NASA polynomials in this model (McBride and Gordon 1967), so that the expression for the molal enthalpy of each species has the form

$$\frac{\bar{h}_i}{RT} = a_1 + \frac{a_2}{2}T + \frac{a_3}{3}T^2 + \frac{a_4}{4}T^3 + \frac{a_5}{5}T^4 + \frac{a_6}{T} \tag{7}$$

where $R$ is the universal gas constant. The specific internal energy of the mixture can then be written as

$$\varepsilon = \sum_{i=1}^{N} R_i Y_i \left\{ a_{6,i} + (a_{1,i} - 1)T + \sum_{k=2}^{5} \frac{a_{k,i}}{k} T^k \right\} \tag{8}$$

where $R_i$ is the gas constant for species $i$.

During a hydrodynamic time step $\Delta t$, combustion is assumed to occur at constant volume, hence both the density and internal energy in a computational cell remain constant during the time step. The reaction progress variable $\lambda$ may change however, indicating that the mixture composition is changing and the temperature is increasing. The new temperature is obtained by solving the following equation using a Newton-Raphson iterative technique:

$$\varepsilon(\lambda^{\mathrm{new}}, T_{\mathrm{new}}) = \varepsilon(\lambda^{\mathrm{old}}, T_{\mathrm{old}})\,. \tag{9}$$

The updated molecular mass is also computed using the new value of $\lambda$ and the pressure is then calculated from the perfect gas law. The advantage of this model is that the only input parameters required are the initial reactant composition and the final product composition. The reference enthalpy is chosen to include the enthalpy of formation. Tonello (1996) has performed a series of one-dimensional detonation calculations using this model and shown that the simulated detonation profiles, pressures, and velocities are in excellent agreement with results calculated using the simple ZND theory.

## 3 Numerical solution

The simulations are based on solutions of the time-dependent Euler equations using the Flux-Corrected Transport (FCT) technique (Boris et al. 1993), an explicit, nonlinear finite difference technique for solving generalized continuity equations. These equations describe the conservation of mass, momentum and energy and have the form

$$\frac{\partial \rho}{\partial t} + \nabla \cdot (\rho \mathbf{v}) = 0 \tag{10}$$

$$\frac{\partial (\rho \mathbf{v})}{\partial t} + \nabla \cdot (\rho \mathbf{v}\ \mathbf{v}) = -\nabla P \tag{11}$$

$$\frac{\partial E}{\partial t} + \nabla \cdot (E \mathbf{v}) = -\nabla (P \mathbf{v}) \quad . \tag{12}$$

Here $\rho$ is the density, $\mathbf{v}$ the fluid velocity, $P$ the pressure, and $E$ the total energy per unit volume, which is given by the following expression

$$E = \rho\varepsilon + \frac{1}{2}\rho \mathbf{v} \cdot \mathbf{v} \quad . \tag{13}$$

The chemistry is included by writing Eqs. (2) and (3) for $f$ and $\lambda$ in terms of the substantial or material derivative and then combining them with the continuity equation, equation (10). The equations for $f$ and $\lambda$ then have the form

$$\frac{\partial (\rho f)}{\partial t} + \nabla \cdot (\rho f \mathbf{v}) = \frac{\rho}{\tau(T, P)} \tag{14}$$

$$\frac{\partial(\rho\lambda)}{\partial t} + \nabla \cdot (\rho\lambda \mathbf{v}) = -\rho \frac{\mathrm{d}\lambda}{\mathrm{d}t} \quad . \tag{15}$$

Equations (10) through (15) are then solved using operator splitting techniques and the LCPFCT algorithm (Oran and Boris 1987).

The computational grid simulates the region of the detonation tube where the detonation in the upper section of the tube reaches the end of the splitter plate and comes into contact with the explosive in the lower section of the tube. This section was modelled using a two dimensional rectangular Cartesian grid. The grid spacing was uniform with $\Delta x = \Delta y = 0.01$ cm, and the time step was limited to 1/4 of the value given by the Courant condition, giving an average time step of $1.0\times10^{-8}$ s. To minimize computational time, all the calculations were initiated on a 320×320 grid, and as the detonation front expanded the grid was successively enlarged through 640×640, 960×960, and 1280×1280.

## 4 Initiating detonation structure

The calculations were initiated from detonation profiles in a 3.2 cm wide channel with a well-defined two dimensional transverse-wave structure. The profiles were developed by perturbing a planar detonation front, and then allowing it to propagate for several thousand time steps. These calculations were initially performed on a 320×960 grid using $\Delta x = \Delta y = 0.01$ cm, and the cellular structure was induced by placing a number of localized high-pressure regions downstream of the planar front. Tonello (1996) has previously performed two-dimensional simulations using the constant reaction rate function F (from Table 1) on a coarse grid ($\Delta x = \Delta y = 0.02$) and found no evidence of reignition. The initiating detonation was planar in this case, but the simulations showed no evidence of cellular structure developing in the diffracted waves. Hence we did not consider function F further, and concentrated on examining the cellular structure produced by the remaining rate functions.

Experimental evidence (Lee et al. 1982, Zitoun et al. 1995) suggests that the detonation cell size in stoichiometric $H_2$-$O_2$ is approximately 1.5 mm. In our 320×960 grid therefore we expect to see approximately 20 detonation cells. However, computations using reaction rate function E produced no long term cellular structure. Detonation cells could be induced initially, but the number of cells was directly related to the number of perturbation sites, and the cellular structure decayed to a planar detonation over several hundred times steps. Using rate functions B and C in calculations did produce cellular structure which persisted, but the number of detonation cells formed initially again appeared to be related to the initial number of perturbation cells rather than converging to the number of cells characteristic of the $H_2$-$O_2$ mixture under consideration. It is possible that if the simulations had been run for longer then the dependence of the detonation cell size on the number of initiating sites may have disappeared. For functions B and C the cellular structure which developed was highly irregular, and the number of triple points on the grid was continuously changing. This is consistent with the behavior expected from $H_2$-$O_2$ systems at atmospheric pressure, where the cellular structure is known to be highly irregular.

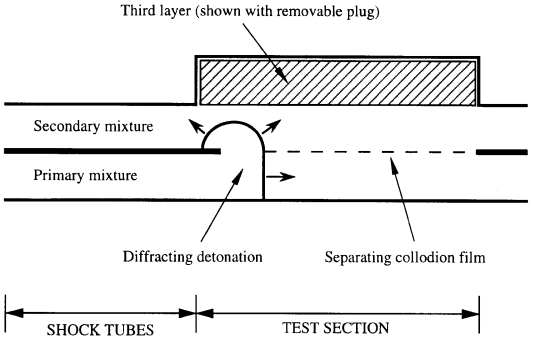


**Fig. 1.** Schematic of special shock tubes for layered detonations

Reaction rate function $D$ provided the most appropriate transverse wave structure. When the detonation front was perturbed by either 1, 4, 7 or 13 high pressure regions, it evolved into a system that always contained approximately 14 quasi-regular detonation cells. This indicates a detonation cell size of approximately 2 mm, which is in reasonable agreement with the experimental results. To initiate the first calculation described in the next section, we used the detonation structure generated from one of these runs. The detonation tube used in the experiments of Liu et al. (1987, 1988) and Tonello at al. (1995) consisted of two 1.6 cm square tubes laid horizontally on top of each other, ending in a test section in which the middle wall has been removed to allow the detonation in the upper tube to interact with the gas in the lower tube, as shown schematically in Fig. 1. To simulate the interaction in the test section, we again used a 320×960 grid and initiated the calculation by overlaying a small segment of the established detonation structure calculated above. This gave an initiating detonation containing approximately seven quasi-regular detonation cells across the upper chamber of the detonation tube.

To provide a different initiating structure, we also perturbed the planar detonation front (again using reaction rate function $D$) using nine high-pressure regions and stopped the calculation before a regular structure had developed. This gave a detonation front with approximately ten highly irregular detonation cells across the front. We used one half of the transverse extent of this detonation front to initiate the second run, described in detail in Sect. 5.2.

## 5 Results

### 5.1 Reignition via triple point collisions

Figure 2 shows pressure contours after 8 $\mu$s. The initiating detonation had a quasi-regular transverse-wave structure containing 14 triple points and producing approximately seven detonation cells. It shows the pressure field after

the first four triple points have expanded over the edge of the splitter plate. By this time, the high-pressure region around the first triple point from the plate has been greatly reduced by the expansion and has virtually disappeared, although some weak high-pressure regions from the remnants of the second triple point are still visible. The third triple point is still moving along the edge of the expanding shock front and is maintaining a concentrated region of relatively high pressure. The fourth triple point has also moved into the lower chamber and created a second high-pressure region which is also moving along the expanding shock front. The fifth triple point is just about to expand into the lower half of the grid.

Figure 3 shows pressure contours for the same calculation after 13 $\mu$s (note that the calculation is now running on a 640×640 grid). The high pressure region from the third triple point has all but disappeared, but the high pressure regions from the fourth and fifth triple points are growing and merging. In addition, the sixth triple point has moved rapidly along the expanding shock front and has begun to merge with the high pressure region from the fifth triple point. This has resulted in the production of another localized high pressure region in close proximity to those already in existence from the movement of the fourth and fifth triple points along the expanding front. This coalescence of high-pressure regions causes the reignition of the detonation.

Figure 4 shows pressure contours after 18.0 $\mu$s, confirming that the detonation is definitely reigniting. The detonation is moving back towards the primary detonation in the upper chamber, and some of the larger regions of the reignited detonation front are beginning to break up into a new cellular structure.

Figure 5 shows the pressure contours after 28.0 $\mu$s (the calculation is now running on a 960×960 grid). The detonation has now completely reignited and is established along the entire front. The reignited detonation along the expanding front has recombined with the primary detonation in the upper channel and the detonation front has broken up into cells characteristic of the stoichiometric $H_2$-$O_2$ mixture.

The behavior described above closely agrees with the experimental observations of Liu et al. (1988) and Tonello et al. (1995) when both the primary and secondary explosive layers are stoichiometric $H_2$-$O_2$. In each of these experiments the cells from the primary, initiating mixture move into the bounding mixture after the primary detonation passes the splitter plate so that a detonation is rapidly established across both the primary and bounding explosive layers.

### 5.2 Reignition via hot spot coalescence

The initiating detonation for this run had a quasi-regular transverse-wave structure that produced only five detonation cells. Figure 6 shows the pressure contours after 18.0 $\mu$s. The structure of the contours in the lower half of the grid is quite different for this calculation. There is no coalescence of high-pressure regions as a result of triple-point interactions, and the pressure field in the expanding front is much more uniform and weaker than the corresponding pressure contours for the previous case. The temperature contours (Fig. 7, on a 960×960 grid after 19.7 $\mu$s) show both the decaying shock front and the contact surface. The very irregular shape of the contact surface is created by the passage of the transverse waves as they expand over the edge of the splitter plate. The temperature contours also show the birth of a small hot spot located on the edge of the expanding front. Comparison of temperature and pressure contours shows that this hot spot originates in a region containing pockets of gas at pressures higher than the "background" pressure, but considerably lower than that of the triple points. These pockets are left over from the expansion of the transverse waves.

Figure 8 (temperature contours after 23.0 $\mu$s) shows that the first ignited hot spot has continued to grow, and then coalesced with a second hot spot formed just above the first hot spot. After 28 $\mu$s (Fig. 9), another hot spot has formed very close to the first two, and all three have grown and merged to create the ignition source seen on the edge of the shock front. This reaction continues to grow, and, after a further 10 $\mu$s, results in almost complete reignition of the detonation along the expanding front. This is shown in the temperature contours in Fig. 10.

### 5.3 Effect of computer precision on transverse wave structure

The transverse-wave structure of the initiating detonation is crucial to the reignition processes occurring in the simulations discussed above. We have repeated these calculations in both single and double precision using initial detonation fronts with no transverse-wave structure. For the single-precision case, reignition of detonation finally occurred, but only because residual numerical noise created sufficient perturbations to the shock front that transverse waves eventually developed. Figure 11 shows temperature contours after 17.0 $\mu$s. A very weak cellular structure is evident behind the detonation front in the upper tube, and several hot spots form on the edge of the shock front. Two of these were formed several microseconds earlier and are about to coalesce. The third, slightly above them, has just been created. Figure 12, temperature contours after a further 11 $\mu$s, shows that the hot spots have continued to grow and reignite the detonation.

The role of numerical noise in the initiation of cellular structure in a planar detonation front has also been observed by Gamezo et al. (1997), and in fact has been used by them as a standard procedure for generating two-dimensional cellular detonations. Schoffel et al. (1988) have also used a similar method for triggering the formation of detonation cells.

The calculation was then repeated in double precision, which considerably delayed the development of the cellular structure. In this case, the detonation did not reignite during the calculation. Figure 13 shows temperature contours for this case at the same time (28 $\mu$s) as the contours shown in Fig. 12. Again, there are very weak transverse

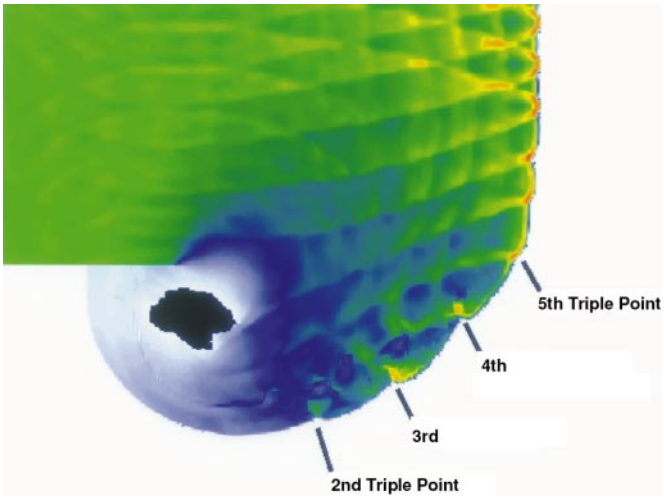


**Fig. 2.** Pressure contours for the first run on a 320×320 grid after 8.0 $\mu$s

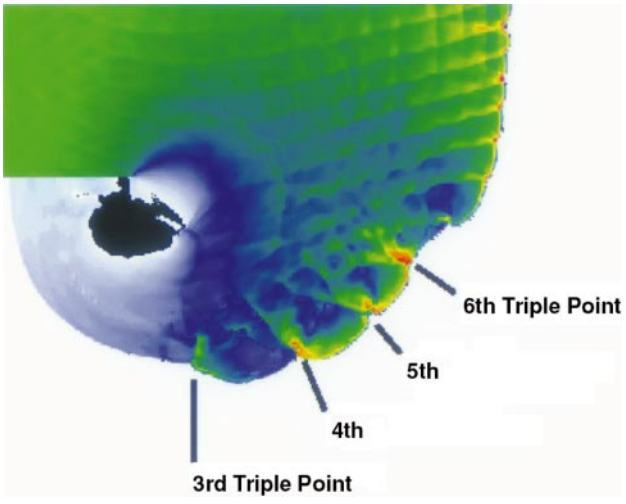


**Fig. 3.** Pressure contours for the first run on a 640×640 grid after 13.0 $\mu$s

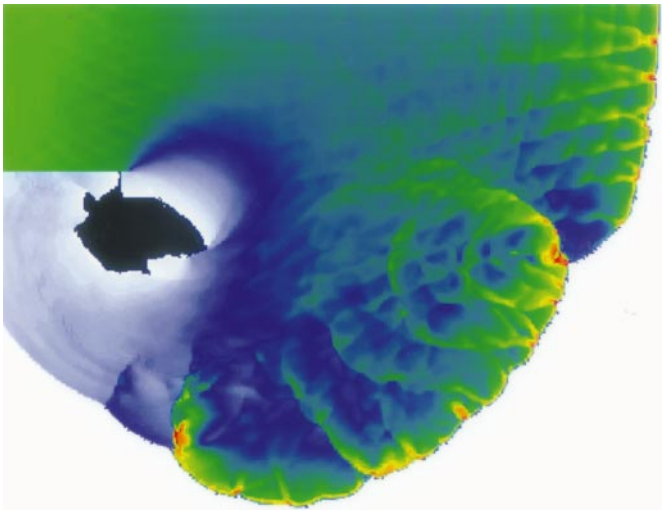

**Fig. 4.** Pressure contours for the first run on a 640×640 grid after 18.0 $\mu$s.

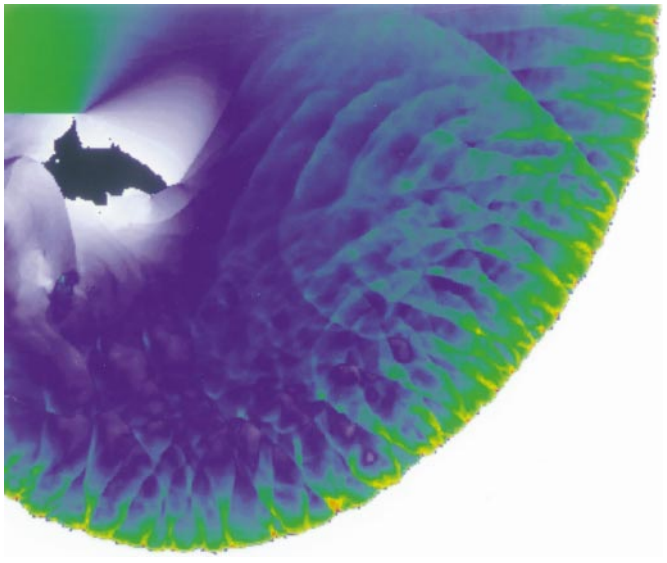

**Fig. 5.** Pressure contours for the first run on a 960×960 grid after 28.0 $\mu$s

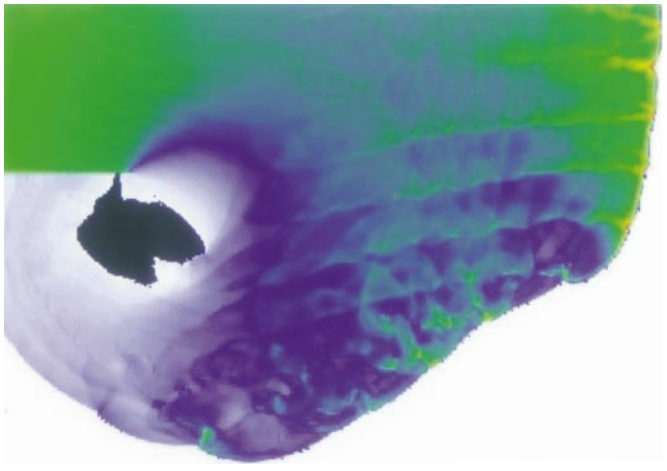

**Fig. 6.** Pressure contours for the second run on a 640×640 grid after 18.0 $\mu$s

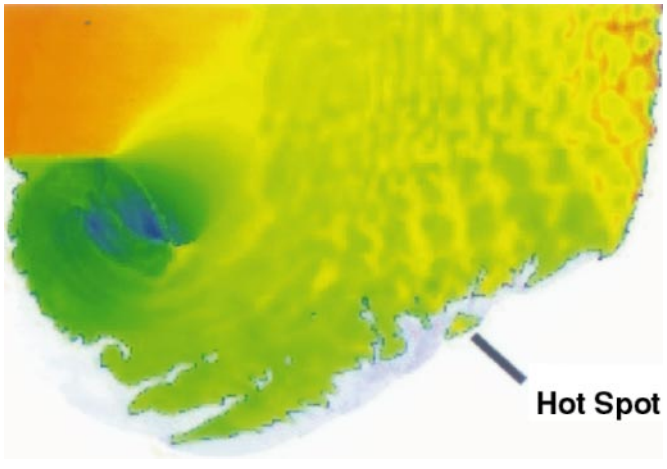


**Fig. 7.** Temperature contours for the second run on a 960×960 grid after 19.7 $\mu$s

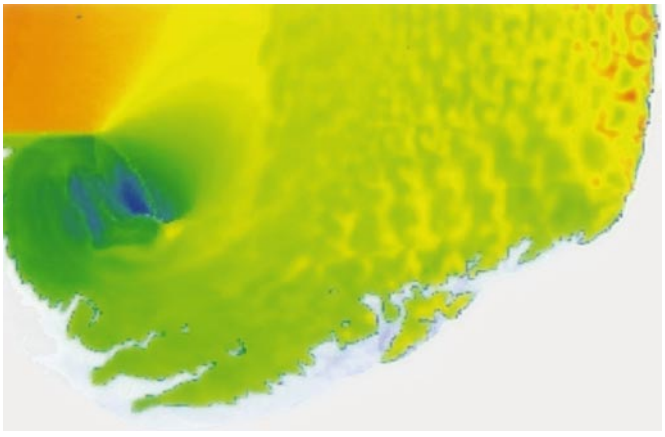

**Fig. 8.** Temperature contours for the second run on a 960×960 grid after 23.0 $\mu$s

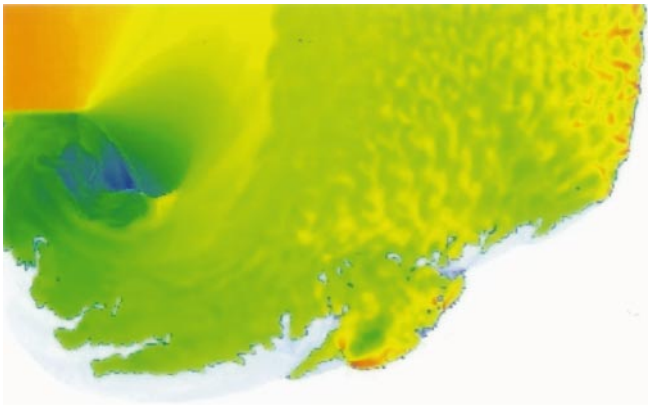

**Fig. 9.** Temperature contours for the second run on a 960×960 grid after 28.0 $\mu$s

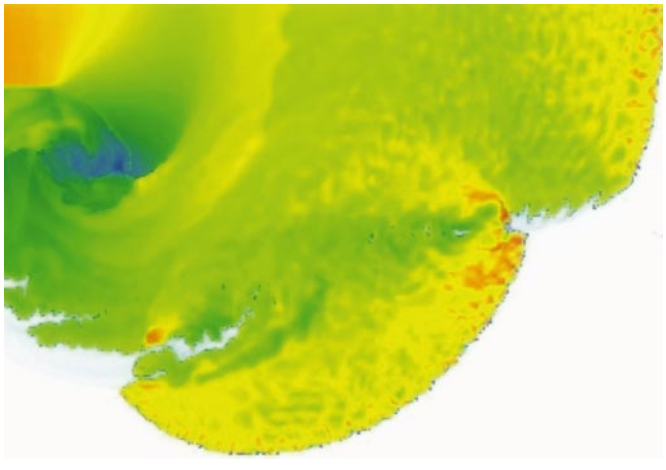

**Fig. 10.** Temperature contours for the second run on a 1280×960 grid after 38.0 $\mu$s

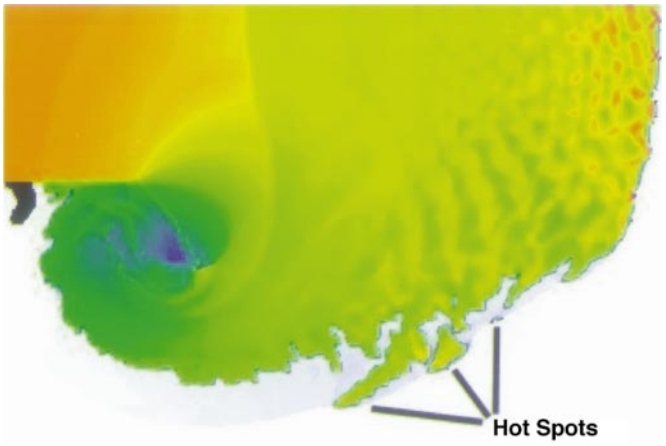


**Fig. 11.** Temperature contours for the third run on a 640×640 grid after 17.0 $\mu$s

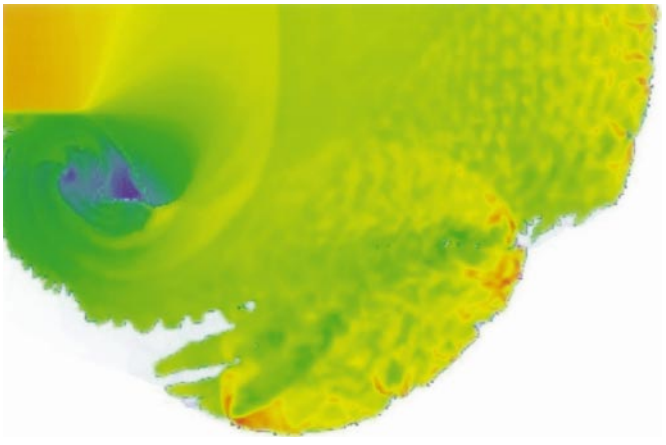

**Fig. 12.** Temperature contours for the third run on a 960×960 grid after 28.0 $\mu$s

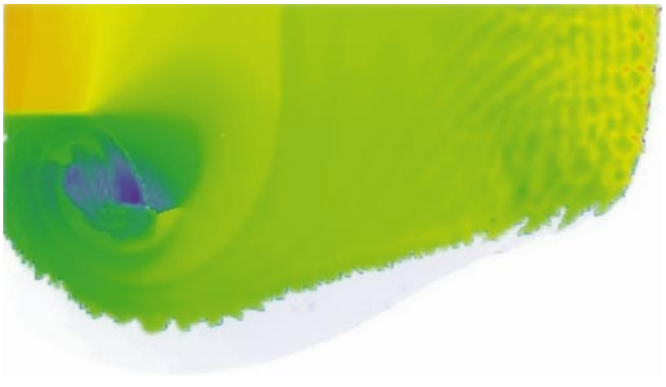

**Fig. 13.** Temperature contours for the fourth run on a 960×960 grid after 28.0 $\mu$s

waves behind the primary detonation, but the flow behind the expanding front is very uniform. No hot spots have formed. This result is very similar to that observed experimentally by Liu et al. (1988) when a 30 nm film was placed between the primary and secondary mixtures in order to block the transmission of transverse waves into the bounding secondary mixture.

## 6 Discussion

Pantow et al. (1996) have also used two-dimensional numerical simulations to study detonation failure and reinitiation associated with sudden expansions. They solved the Euler equations using a two step MacCormack scheme and used a flux-corrected transport algorithm to handle strong shocks. A two-step parameter model was used to represent the chemical kinetics, and the model simulated the behavior of $H_2$-$O_2$ mixtures diluted by different amounts of argon or nitrogen. Their calculations contained sufficient resolution to resolve the cellular structure of the detonation front, and all simulations were initiated by a planar detonation front having a well defined cellular structure. Their simulations showed examples of detonation failure, reignition of detonation after Mach reflection from confining walls, as well as direct reignition. In the latter case, their simulated schlieren profiles were very similar to the pressure contours shown in Fig. 4, indicating that an explosion had been triggered in the shock-heated material between the shock front and the reaction front, which then created a strongly coupled reactive shock wave which travelled along the curved leading shock and reignited the detonation. These simulations showed that the existence of transverse shock waves in the decoupled reaction zone were essential for the reignition of the detonation front, but the mechanisms by which these transverse waves created the ignition sites was not clearly explained.

Efimenko et al. (1994) have also performed an extensive series of two-dimensional numerical simulations to study the critical tube diameter problem. This refers to the experimental observation that if a planar detonation wave propagating in a circular tube suddenly emerges into an unconfined space containing the same material, then the planar wave will transform into a spherical wave only if the tube diameter $d$ is greater than a certain critical value $d_c$. Otherwise, the detonation fails. Early work by Mitrofanov and Soloukin (1965) noted that the critical tube diameter could be related to the detonation cell size of the mixture ($\lambda$) by the simple formula $d_c = 13\lambda$. The work of Efimenko et al. concentrated on the differences between mixtures displaying regular and irregular cellular structure, and noted that more regular systems appeared to have a smaller value of $d_c$ than irregular systems, which is opposite to the experimental observations. They also noted that the appearance of a strong local explosion in a reaction zone was much more probable in irregular systems compared to regular ones. The mechanism by which the detonation was reignited in either the regular or irregular mixtures was not described however.

In the work of Edwards et al. (1979) and Murray et al. (1983) on the reignition of detonation at an area expansion, the reignition occurs at sites along the expansion wave originating at the area change. The reignition in the numerical simulations presented in this paper are qualitatively different, however. In the results described in Sect. 5.1, reignition occurs because of triple point collisions which take place along the edge of the expanding shock front. In the results described in Sects. 5.2 and 5.3, reignition also takes place on the edge of the expanding shock front. However, in this case the ignition kernel is formed from a number of small hot spots which appear on the shock front and originate from a region containing remnant pockets of gas at pressures higher than the background pressure, but considerably lower than that of the triple points.

The difference in the regularity of the cellular structure may affect the mode by which reignition occurs. Lee (1993) has discussed the critical tube diameter problem in detail, and in particular, its breakdown for mixtures with regular cellular structure. He notes that for mixtures with very irregular cellular structure, for which the $d_c = 13\lambda$ criterion holds, the failure wave occurs at the head of the expansion fan. In this case, reignition is caused by the formation of explosion centers near the failure wave as it propagates towards the charge axis. On the other hand, for mixtures with very regular cellular structure, the failure wave does not correspond to the head of the expansion fan. In these cases, failure occurs due to excessive curvature of the entire detonation front. The cellular structure of the detonations modeled here is "quasi regular." The finite size of the grid acts as a cut off for any high-frequency components. Thus the behavior of the detonations modeled in this paper is probably closer to experimental mixtures described as having "regular" cellular structure.

A qualitative difference between experiment and the simulations presented here is the two-dimensional nature of the calculations. Williams et al. (1996) have recently described the detailed structure of three-dimensional detonations using numerical techniques similar to those used here. The simulations show that, in the absence of wall losses, the three-dimensional cell size is about the same as in two dimensions. The transverse wave structure, however, is much more intricate. Two perpendicular modes exist, which are approximately one-quarter of a period out of phase. The interaction of the two transverse waves results in a vorticity field which is much more complex than in two dimensions, and this enhanced vorticity may provide a new trigger for the production of additional explosion sites.

## 7 Conclusion

The simulations described here provide detailed descriptions of two related mechanisms by which an expanding and decaying detonation front can be directly reignited. The first is the triple point collision method, as described in Sect. 5.1, and is similar to the mechanism identified in $H_2$-$O_2$-Ar by Jones et al. (1996). The second is the hot

spot formation process, described in Sect. 5.2, which appears to be caused by the interaction of remnant pockets of gas at pressures higher than the background pressure, but considerably lower than that of the triple points. The different mechanisms occurred when slightly different detonation profiles were used to initiate the calculations, and show that for such sensitive mixtures as $H_2$-$O_2$, very small variations can result in significant changes in the mode of initiation, both in experiment and numerical simulation.

*Acknowledgements.* This work was presented at the 16th International Colloquium on the Dynamics of Explosions and Reactive Systems in Cracow, Poland. It was sponsored in part by The Office of Naval Research through the Naval Research Laboratory, and in part by The U.S. Army Research Office under grant DAAL03-87-K-009. The authors wish to thank Eric Northeast for considerable assistance with the preparation of the figures.

## References

Boris JP, Landsberg AM, Oran ES, Gardner JH (1993) LCPFCT-A flux-corrected transport algorithm for solving generalized continuity equations. NRL/MR/6410–93-7192, Naval Research Laboratory, Washington, DC

Burks TL, Oran ES (1981) A computational study of the chemical kinetics of hydrogen combustion. NRL Memorandum Report 4446, Naval Research Laboratory, Washington, DC

Edwards DH, Thomas DO, Nettleton MA (1979) The diffraction of a planar detonation wave at an abrupt area change. J Fluid Mech, 95: 79–96

Efimenko AA, Dorofeev SB, Shepherd JE (1994) Chemical reaction kinetics and detonation modelling. In: Proc of 25th Int Symp on Combustion, Irvine, CA, August 1994

Gamezo VN, Desbordes D, Oran ES (1999) Formation and evolution of two-dimensional cellular detonations. Combustion and Flame, 116: 154–165

Jones DA, Kemister, G, Sichel, M, Oran ES (1996) The influence of cellular structure on detonation transmission. Shock Waves, 6: 119–130

Jones DA, Oran ES, Sichel M (1995) Reignition of detonation by reflected shocks. Shock Waves, 5: 47–57

Lee JH (1993) On the critical diameter problem. In: JR Bowen et al. (eds) Dynamics of Exothermicity, Gordon and Breach Publishers, pp 321–335

Lee JHS, Knystautas R, Guirao CM (1982) The link between cell size, critical tube diameter, initiation energy, and detonability limits, in fuel-air explosions. S M Study Series Lee JHS, Guirao CM (eds) University of Waterloo Press, Waterloo, Ontario, Canada, No. 16, pp 157–186

Lefebvre MH, Oran ES, Kailasanath K (1992) Computations of detonation structure: the influence of model input parameters. NRL Memorandum Report 4404-92-6961, Naval Research Laboratory, Washington, DC

Lefebvre MH, Oran ES, Kailasanath K, Van Tiggelen PJ (1993) The influence of the heat capacity and diluent on detonation structure. Combustion and Flame, 95: 206–218

Liu JC, Liou JJ, Sichel M, Kauffman CW, Nicholls JA (1987) Diffraction and transmission of a detonation into a bounding explosive layer. In: Proc of the 21st Int Symp on Combustion, The Combustion Institute, Pittsburgh, pp 1659–1668

Liu JC, Sichel M, Kauffman CW (1988) The lateral interaction of detonating and detonable gas mixtures. Progress in Astronautics and Aeronautics, 114: 264–283

Mitrofanov VV, Soloukhin RI (1965) The diffraction of multifront detonation waves. Sov Phys-Dokl, 9: 1055

Murray SB, Lee JH (1983) On the transformation of planar detonation to cylindrical detonation. Combustion and Flame, 52: 269–289

Meyer JW, Oppenheim AK (1971) On the shock-induced ignition of explosive gases. In: Thirteenth Explosion (International) on Combustion, The Combustion Institute, Pittsburgh, pp 1153

Oran ES, Boris JP (1987) Numerical simulation of reactive flow. Elsevier Publishing Co Inc

Oran ES, Jones DA, Sichel M (1992) Numerical simulations of detonation transmission. Proc Roy Soc Lond A, 436: 267–297

Oran ES, Weber JW Jr, Stefaniw EI, Lefebvre MH (1998) A numerical study of a two-dimensional $H_2$-$O_2$-Air detonation using a detailed chemical reaction model. Combustion and Flame, 113: 147–163

Pantow EG, Fischer M, Kratzel Th (1996) Decoupling and recoupling of detonation waves associated with sudden expansion. Shock Waves, 6: 131–137

Schoffel SU, Ebert F (1988) AIAA Progr Astron Aeronautics, 114: 3–31

Taki S, Fujiwara T (1981) Numerical simulation of triple shock behavior of gaseous detonation. In: Eighteenth Int Symp on Combustion, The Combustion Institute, Pittsburgh, PA, pp 1671–1681

Tonello A, Sichel, M, Oran ES (1996) Numerical simulations of the diffraction of planar detonations in $H_2$-$O_2$ mixtures. In: Proc of the 26th Int Symp on Combustion, The Combustion Institute, Pittsburgh, PA, pp 3033–3039

Tonello NA (1996) An experimental and computational study of the mechanisms of detonation transmission in layered $H_2$-$O_2$ mixtures. PhD thesis, The University of Michigan

Tonello NA, Sichel M, Oran ES (1995) A simplified kinetic model for detonations in $H_2$-$O_2$. In: 15th International Colloquium on the Dynamics of Explosions and Reactive Systems, Boulder, CO, August, 1995

Weber J (1994) Physical and numerical aspects of two dimensional detonation simulations including detailed chemical kinetics on a massively parallel connection machine. Ph. D. Thesis, The University of Maryland, College Park, Maryland

Westbrook CK (1982) Hydrogen oxidation kinetics in gaseous detonations. Combustion Science and Technology, 29: 615–623

Williams DN, Bauwens L, Oran ES (1996) Detailed structure and propagation of three-dimensional detonations. In: Proc of the 26th Int Symp on Combustion, The Combustion Institute, Pittsburgh, PA, pp 2991–2998

Zitoun R, Desbordes D, Guerraud C, Deshaies B (1995) Direct initiation of detonation in cryogenic gaseous $H_2$-$O_2$ mixtures. Shock Waves, 4: 331–337